The acyltransferase LYCAT controls specific phosphoinositides and related membrane traffic

Leslie N. Bone[a,b], Roya M. Dayam[a,b], Minhyoung Lee[c], Nozomu Kono[d], Gregory D. Fairn[c,e], Hiroyuki Arai[d,f], Roberto J. Botelho[a,b,*], and Costin N. Antonescu[a,b,e,*]

[a]Department of Chemistry and Biology and [b]Graduate Program in Molecular Science, Ryerson University, Toronto, ON M5B 2K3, Canada; [c]Department of Biochemistry, University of Toronto, Toronto, ON M5S 1A8, Canada; [d]Department of Health Chemistry, Graduate School of Pharmaceutical Sciences, University of Tokyo, Tokyo 113-0033, Japan; [e]Keenan Research Centre for Biomedical Science of St. Michael's Hospital, Toronto, ON M5B 1W8, Canada; [f]Japan Agency for Medical Research and Development–Core Research for Evolutionary Science and Technology, Tokyo 113-0033, Japan

ABSTRACT **Phosphoinositides (PIPs) are key regulators of membrane traffic and signaling. The interconversion of PIPs by lipid kinases and phosphatases regulates their functionality. Phosphatidylinositol (PI) and PIPs have a unique enrichment of 1-stearoyl-2-arachidonyl acyl species; however, the regulation and function of this specific acyl profile remains poorly understood. We examined the role of the PI acyltransferase LYCAT in control of PIPs and PIP-dependent membrane traffic. LYCAT silencing selectively perturbed the levels and localization of phosphatidylinositol-4,5-bisphosphate [PI(4,5)P_2] and phosphatidylinositol-3-phosphate and the membrane traffic dependent on these specific PIPs but was without effect on phosphatidylinositol-4-phosphate or biosynthetic membrane traffic. The acyl profile of PI(4,5)P_2 was selectively altered in LYCAT-deficient cells, whereas LYCAT localized with phosphatidylinositol synthase. We propose that LYCAT remodels the acyl chains of PI, which is then channeled into PI(4,5)P_2. Our observations suggest that the PIP acyl chain profile may exert broad control of cell physiology.**

Monitoring Editor
John York
Vanderbilt University

Received: Sep 19, 2016
Revised: Oct 24, 2016
Accepted: Nov 1, 2016

INTRODUCTION

Phosphoinositides (PIPs) control many facets of cell physiology, such as nutrient uptake, receptor signaling, and cell adhesion by control of specific stages of membrane traffic (Di Paolo and De Camilli, 2006; Krauss and Haucke, 2007). Through the action of lipid kinases and phosphatases, PIPs can be interconverted into seven different species defined by phosphorylation of the inositol head group (Balla, 2013). Each of the seven PIPs exhibits unique enrichment within membrane compartments and helps to recruit a variety of cognate effector proteins. Phosphatidylinositol-4,5-bisphosphate (PI(4,5)P_2) and phosphatidylinositol-3-phosphate (PI(3)P) illustrate these concepts well.

PI(4,5)P_2 predominates within the plasma membrane (PM) and regulates clathrin-mediated endocytosis (referred to here as endocytosis) to control the internalization of cell surface proteins such as transferrin (Tfn) receptor (TfR; Jost *et al.*, 1998; Varnai *et al.*, 2006; Zoncu *et al.*, 2007; Posor *et al.*, 2013). PI(4,5)P_2 binds to and recruits AP2 and other proteins, which, together with cargo molecules and clathrin, initiate the formation and assembly of clathrin-coated pits (CCPs; Gaidarov and Keen, 1999; Itoh *et al.*, 2001; Jackson *et al.*, 2010). CCPs couple cargo selection to membrane invagination and eventually undergo scission from the PM by the GTPase dynamin2 to yield endocytic vesicles (Conner and Schmid, 2003; McMahon and Boucrot, 2011). CCPs harbor lipid phosphatases such as synaptojanins and OCRL that mediate PI(4,5)P_2 turnover to control the efficiency of vesicle formation (Antonescu *et al.*, 2011) and, after

This article was published online ahead of print in MBoC in Press (http://www.molbiolcell.org/cgi/doi/10.1091/mbc.E16-09-0668) on November 9, 2016.

*Address correspondence to: Roberto J. Botelho (rbotelho@ryerson.ca), Costin N. Antonescu (cantonescu@ryerson.ca).

Abbreviations used: CCP, clathrin-coated pit; CDP, cytidine diphosphate; CDS, cytidine diphosphate-diacylglycerol synthase; CL, cardiolipin; DAG, diacylglycerol; eGFP-CLCa, enhanced green fluorescent protein fusion of clathrin light chain a; HPLC, high-performance liquid chromatography; LC-ESI-MS/MS, liquid chromatography–electrospray ionization mass spectrometry; LCS, localization correlation score; LYCAT, lysocardiolipin acyltransferase; PA, phosphatidic acid; PI, phosphatidylinositol; PI(3)P, phosphatidylinositol-3-phosphate; PI(4)P, phosphatidylinositol-4-phosphate; PI(4,5)P_2, phosphatidylinositol-4,5-bisphosphate; PIP, phosphoinositide; PIP_1, monophosphorylated PIP; PIP_2, bisphosphorylated PIP; PIPKI, type I phosphatidylinositol phosphate kinase; PIS, phosphatidylinositol synthase; PM, plasma membrane; RPE, retinal pigment epithelial cells; Tfn, transferrin; TfR, transferrin receptor; TIRF-M, total internal reflection fluorescence microscopy; VSVG, vesicular stomatitis virus G.

scission, clathrin uncoating (Cremona *et al.*, 1999; Kim *et al.*, 2002). Disruption of PI(4,5)P_2 synthesis and turnover affects CCP initiation, size, and lifetime (Cremona *et al.*, 1999; Nakatsu *et al.*, 2010; Antonescu *et al.*, 2011; Posor *et al.*, 2013; Nández *et al.*, 2014).

Endocytic vesicles traffic to early endosomes, which sort and send cargo molecules to specific destinations such as to the lysosomes for degradation or recycling to the PM, processes that require PI(3)P (Li *et al.*, 1995; Puchner *et al.*, 2013). PI(3)P binds to and recruits effector proteins like EEA1, which mediate endosome fusion, and sorting nexins, which mediate cargo sorting and vesiculation. To complete recycling of internalized cargo to the PM, PI(3)P is then dephosphorylated to phosphatidylinositol (PI) by myotubularin-1 (Ketel *et al.*, 2016). Hence the internalization, sorting, and trafficking of membrane cargo proteins depends on the dynamic and sequential interconversion of PIP species by coordinated regimes of phosphorylation and dephosphorylation.

Although much has been revealed about the regulation and function of PIPs based on modification of the inositol head group, much less is known about the control and function of the acyl chains of these lipids, despite the fact that 50–70% of total PI is 1-stearoyl-2-arachidonyl (18:0/20:4, combined as 38:4), an acyl chain enrichment not found in other phospholipids (Holub and Kuksis, 1978; Hicks *et al.*, 2006; Imae *et al.*, 2011; D'Souza and Epand, 2014). In addition, PIPs also exhibit many minor acyl combinations, generating a great molecular diversity that remains functionally unexplored. PIP acyl chains are likely to affect regulation and function because acyl chains affect the substrate preference of type I phosphatidylinositol phosphate kinases (PIPKI) and OCRL, which synthesize and degrade PI(4,5)P_2, respectively (Schmid *et al.*, 2004; Shulga *et al.*, 2012).

Acyl chain specificity and diversity may arise during de novo synthesis of PI in the endoplasmic reticulum (ER), where one of many acyltransferases may add acyl chains to generate the biosynthetic precursor phosphatidic acid (PA), which then is converted to cytidine diphosphate (CDP)–diacylglycerol (DAG) by CDP-diacylglycerol synthase (CDS; D'Souza and Epand, 2014). CDS2 shows preference for 38:4 PA, which may then be channeled to PI synthase (PIS; D'Souza *et al.*, 2014; D'Souza and Epand, 2015). Alternatively, PI/PIP acyl chains may be remodeled postsynthesis by the action of phospholipases and acyltransferases (Shindou and Shimizu, 2009; Imae *et al.*, 2011; Kim *et al.*, 2011). However, there is a dearth of knowledge about these PI acyltransferases.

Lysocardiolipin acyltransferase (LYCAT; also known as LCLAT1 or ALCAT1) is a lipid acyltransferase that exhibits preference for lysophosphatidylinositol and lysophosphatidylglycerol over other phospholipids in vitro, as well as preference for incorporating longer fatty acyl-CoA substrates (18:0,18:1 over 12:0,16:0) into these lysolipids (Zhao *et al.*, 2009). LYCAT-knockout mice exhibit a reduction of stearate and an increase in palmitate within PI/PIPs in various tissues (Imae *et al.*, 2011). Taken together, these studies show that LYCAT is required for PI/PIP acyl chain specificity, perhaps by selectively incorporating stearate into the *sn-1* position of PI/PIPs. Indeed a similar role has been proposed for the *Caenorhabditis elegans* homologues of LYCAT (Imae *et al.*, 2010, 2011). LYCAT may also remodel the acyl chain profile of cardiolipin (CL; Cao *et al.*, 2004). In mice fed a high-fat diet as a model of diet-induced obesity, LYCAT expression is enhanced, leading to CL acyl remodeling and mitochondrial defects (Li *et al.*, 2010). LYCAT-knockout mice are protected from defects in mitochondrial function and insulin signaling induced by high-fat feeding (Li *et al.*, 2010). Given that LYCAT-knockout mice fed a normal diet exhibited only reduced stearate content within PI without changes in other lipids (including CL; Imae *et al.*, 2011), it is likely that the predominant function of LYCAT under normal conditions is to control PI/PIP acyl chain profile.

Although LYCAT regulates the acyl chain profile of PI/PIPs and CL, the function of LYCAT in controlling membrane traffic remains unexplored. Using biochemical and lipidomic measurements to quantify lipids and lipid acyl species in combination with microscopy-based approaches to resolve how perturbations of LYCAT affect endomembrane traffic, we find that LYCAT exerts control over the acyl chain profile of specific PIP species and has an important but selective role in regulating multiple aspects of PIP-dependent endomembrane traffic.

RESULTS

LYCAT silencing perturbs endosomal traffic but not biosynthetic traffic

To examine whether LYCAT controls PIP-dependent endomembrane traffic, we used small interfering RNA (siRNA)–mediated silencing of LYCAT in human ARPE-19 cells (RPE henceforth), which resulted in an ~80% reduction in LYCAT protein expression (Supplemental Figure S1, A and B), and examined TfR membrane traffic, a process controlled by PI(4,5)P_2-dependent endocytosis (Varnai *et al.*, 2006), and PI(3)P-dependent intracellular traffic (van Dam *et al.*, 2002). LYCAT silencing significantly reduced cell surface TfR levels (Figure 1, A and B), whereas total levels of TfR were unaltered (Supplemental Figure S1, C and D). Of importance, cell surface TfR levels in LYCAT-silenced cells were rescued by expression of siRNA-resistant exogenous LYCAT, demonstrating that the altered surface levels of TfR were due to specific perturbation of LYCAT (Figure 1C).

TfR exhibits a pronounced perinuclear morphology as a result of trafficking through intracellular compartments, including recycling endosomes (Dugani *et al.*, 2008). LYCAT silencing caused a dispersal of the perinuclear accumulation of TfR (Figure 1, D and E), further suggesting a major perturbation of intracellular trafficking upon LYCAT silencing. To contrast with endocytic trafficking, we examined the biosynthetic membrane traffic pathway, which is controlled by phosphatidylinositol-4-phosphate (PI(4)P; Szentpetery *et al.*, 2010), using a temperature-sensitive form of vesicular stomatitis virus G (VSVG) that is trapped in and then released from the ER by temperature shift (Presley *et al.*, 1997; Szentpetery *et al.*, 2010). LYCAT silencing did not alter VSVG trafficking and distribution (Figure 1, F and G). Thus LYCAT silencing alters TfR traffic, which relies on PI(4,5)P_2 and PI(3)P, but has no apparent effect on the PI(4)P-dependent biosynthetic pathway.

LYCAT silencing reduces total levels and alters localization of PI(3)P and PI(4,5)P_2

Defective TfR distribution in LYCAT-silenced cells might correspond to altered PIP levels, which we tested by labeling cells with [^{3}H]myo-inositol and measuring the levels of specific PIPs by high-performance liquid chromatography (HPLC; Ho *et al.*, 2016). LYCAT silencing reduced the levels of PI(3)P and PI(4,5)P_2 by 25% ± 0.05% and 21% ± 0.06%, respectively, but had no effect on PI(4)P levels (Figure 2A), suggesting that LYCAT silencing affects the levels of a subset of PIPs and associated functions.

We then examined the cellular localization of PIPs, using fluorescently labeled protein probes specific for PI(3)P, PI(4)P, and PI(4,5)P_2 (Stauffer *et al.*, 1998; Stenmark *et al.*, 2002; Hammond *et al.*, 2014). LYCAT silencing reduced the number of 2FYVE-GFP structures, consistent with abated levels of PI(3)P (Figure 2, B and C). LYCAT silencing also altered the localization of the PI(4,5)P_2 probe PH-PLCδ-GFP (Várnai and Balla, 1998). Whereas in control cells, PH-PLCδ-GFP predominantly and uniformly decorated the PM, in LYCAT-silenced

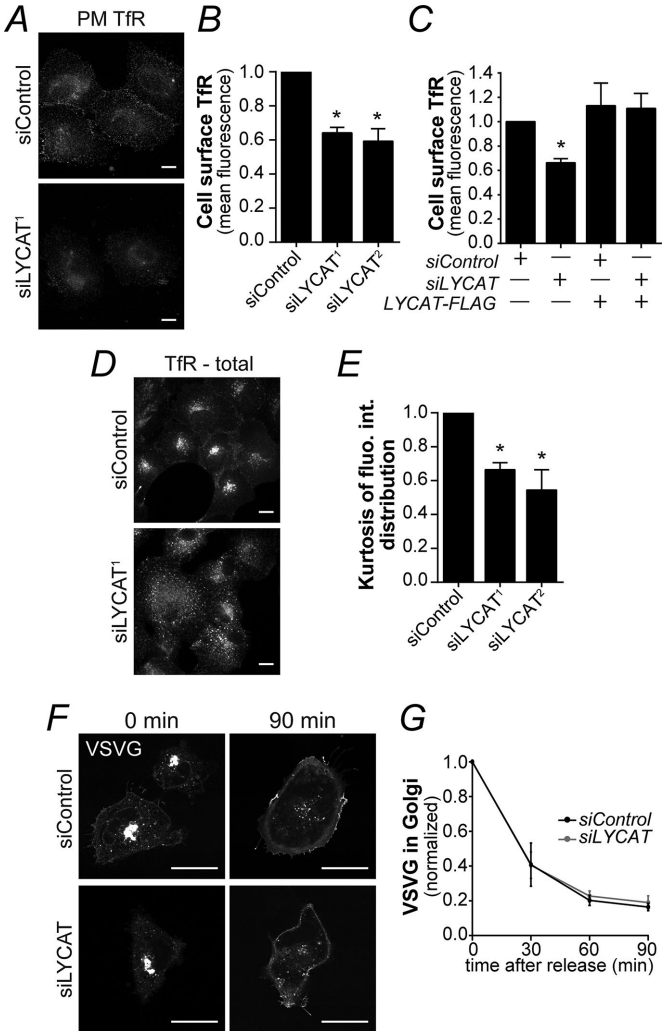

FIGURE 1: LYCAT silencing perturbs endomembrane traffic but not biosynthetic traffic. RPE cells were transfected with one of two distinct siRNA sequences targeting LYCAT (siLYCAT[1] or siLYCAT[2]) or nontargeting siRNA (siControl). (A, B) Detection of cell surface TfR levels by immunofluorescence staining of intact (nonpermeabilized) cells. (A) Representative epifluorescence micrographs (scale bar, 20 μm). (B) Mean cell surface TfR ± SEM from at least four independent experiments. *$p < 0.05$. (C) After silencing, cells were transfected with a cDNA encoding LYCAT-FLAG, followed by detection of cell surface TfR levels by immunofluorescence staining of intact cells; mean cell surface TfR ± SEM ($n = 4$), *$p < 0.05$. (D, E) Detection of total cellular TfR levels (permeabilized cells). (D) Representative epifluorescence micrographs (scale bar, 20 μm) and (E) quantitative measurements (mean ± SEM) of the relative concentration of TfR staining within the perinuclear region ($n = 4$), *$p < 0.05$. (F, G) Measurement of biosynthetic traffic from the Golgi to PM. GFP-VSVG was released from Golgi arrest for indicated times. (F) Representative micrographs (scale bar, 5 μm). (G) Mean ± SEM ($n = 3$) of the amount of VSVG-GFP remaining in the Golgi at various times.

cells, this probe labeled tubular and punctate structures throughout the cell (Figure 2B). In contrast, the localization of the PI(4)P probe P4M-GFP was indistinguishable between control and LYCAT-silenced cells, a distribution consistent with the PM and the *trans*-Golgi network (Hammond *et al.*, 2014; Figure 2B). Collectively these data indicate that LYCAT selectively affects the levels and localization of PI(3)P and PI(4,5)P_2 but not those of PI(4)P.

LYCAT silencing alters clathrin-mediated endocytosis

Because LYCAT silencing altered the levels and localization of PI(4,5)P_2, we next investigated the effect of LYCAT silencing on CCP dynamics, which is controlled by PI(4,5)P_2 (Antonescu *et al.*, 2011). We performed time-lapse total internal reflection fluorescence microscopy (TIRF-M) in RPE cells stably expressing a GFP-fusion of clathrin light chain (eGFP-CLCa; Figure 3A) followed by automated detection, tracking, and analysis of CCPs (Aguet *et al.*, 2013). Consistent with reduction of PI(4,5)P_2 levels and perturbation of PI(4,5)P_2 localization, LYCAT silencing reduced CCP initiation density (Figure 3B) and CCP size (Figure 3C), the latter measured by the fluorescence intensity of eGFP-CLCa within diffraction-limited CCPs. We also observed that LYCAT silencing altered CCP lifetimes (Supplemental Figure S1E). Consistent with these defects in CCP dynamics, we observed that LYCAT silencing led to a significant reduction in the rate of Tfn internalization (Figure 3D). Together these data indicate that LYCAT is a novel regulator of endocytosis, likely by affecting PI(4,5)P_2 levels and localization.

LYCAT silencing alters intracellular traffic of TfR

Because LYCAT suppression reduced PI(3)P levels, we predicted that PI(3)P-dependent trafficking processes would be disturbed in LYCAT-silenced cells. To test this, we monitored the arrival of fluorescently labeled Tfn pulsed for various time points into EEA1-positive endosomes. LYCAT silencing did not appreciably alter the number or intensity of EEA1 puncta, indicating that we could employ EEA1 as a marker of early endosomes (Supplemental Figure S2A). LYCAT silencing substantially delayed the arrival of Tfn to EEA1 compartments (Figure 4, A and B), which is consistent with the effect of reduction in PI(3)P levels by other manipulations (van Dam *et al.*, 2002).

We next investigated whether LYCAT-silenced cells manifested a defect in TfR recycling. First, we measured the ability of internalized Tfn to access the total pool of internal TfR-labeled endosomes, which include recycling endosomes. We observed a delayed arrival of Tfn to the total pool of cellular TfR in LYCAT-silenced cells relative to control cells (Supplemental Figure S2, B and C). To complement this assay and measure the rate of TfR recycling, we treated live cells with antibodies that recognize an exofacial TfR epitope to measure the rate of arrival of TfR to the PM, thus measuring TfR recycling (Antonescu *et al.*, 2008). LYCAT silencing reduced the rate of labeling with anti-TfR antibody (Figure 4C), indicating that TfR recycling is slower in LYCAT-deficient cells. Collectively our studies reveal that LYCAT is necessary for TfR intracellular trafficking, a process that depends on PI(3)P.

LYCAT controls the acyl chain profile of specific PIPs

LYCAT regulates the specific content of stearate within PI/PIPs in mice (Imae *et al.*, 2011), yet LYCAT silencing did not affect PI(4)P levels or secretion from the biosynthetic pathway while abating PI(3)P and PI(4,5)P_2 levels and interfering with endocytic trafficking. To better understand how LYCAT might differentially affect PIPs and trafficking processes, we analyzed the acyl chain composition of various phospholipids using liquid chromatography–electrospray ionization mass spectrometry (LC-ESI-MS/MS). The acyl chain composition of each lipid is presented as a combination of the *sn-1* and *sn-2* acyl groups (e.g., the 1-stearoyl-2-arachidonyl species corresponds to 38:4). As previously reported (Holub and Kuksis, 1978; Hicks *et al.*, 2006; Imae *et al.*, 2011; D'Souza and Epand, 2014), PI shows a unique and striking enrichment for the 38:4 acyl composition that is not seen in other phospholipids (Supplemental Figure S3A). LYCAT silencing did not appreciably disturb the acyl chain

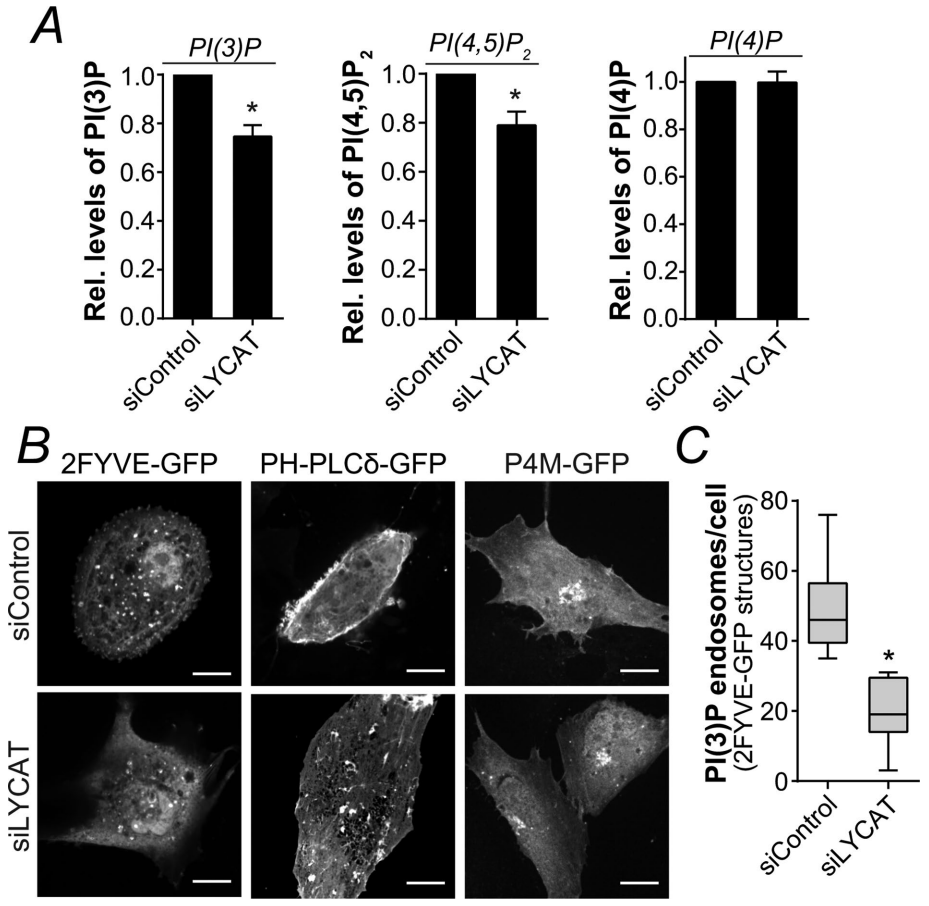

FIGURE 2: LYCAT silencing reduces total levels and alters localization of PI(3)P and PI(4,5)P_2. RPE cells were transfected with siRNA targeting LYCAT (siLYCAT) or nontargeting siRNA (siControl). (A) The levels of PI(3)P, PI(4,5)P_2, and PI(4)P were measured after [^{3}H]myo-inositol labeling, HPLC, and detection by flow scintillation. Mean ± SEM ($n = 4$). (B, C) Cells were also transfected with cDNAs encoding 2FYVE-GFP, PH-PLCδ-GFP, or P4M-GFP to probe for PI(3)P, PI(4,5)P_2, and PI(4)P, respectively. (B) Representative epifluorescence micrographs (scale bar, 20 μm). (C) Median, 25th and 75th percentiles (boxes), and Tukey range (whiskers) of the number of 2FYVE-GFP–positive structures per cell ($n = 3$), *$p < 0.05$.

composition of phosphatidylcholine (PC), phosphatidylethanolamine (PE), and phosphatidylserine (PS; Supplemental Figure S3, B–D). Surprisingly, LYCAT silencing also did not affect the acyl chain profile of total PI (Supplemental Figure S3E).

We surmised that LYCAT may preferentially affect the acyl chain profile of specific PIPs instead. To address this hypothesis, we analyzed the acyl composition of PIP species using phosphate methylation and LC-ESI-MS/MS to resolve PI, monophosphorylated PIPs (PIP_1), and bisphosphorylated PIPs (PIP_2; Clark *et al.*, 2011). Of interest, the acyl chain profile of PI and PIP_1 species, the latter being predominantly PI(4)P, were unaltered in LYCAT-silenced cells (Figure 5, A and B, and Supplemental Figure S4, A and B; Stephens *et al.*, 1993). In contrast, PIP_2, which is mainly PI(4,5)P_2, exhibited reduced levels of many acyl combinations in LYCAT-silenced cells, which partially reflects the reduced PI(4,5)P_2 levels in these cells (Figure 5C and Supplemental Figure S4C). Of importance, we observed a shift in the acyl chain profile in PIP_2 upon LYCAT silencing, as determined by the ratio of 38:*x* to 36:*x* acyl species (where *x* refers to any level of unsaturation). In contrast to the altered acyl chain profile of PIP_2, the 38:*x* to 36:*x* ratios of PI and PIP were unaffected by LYCAT silencing (Figure 5D). These findings are consistent with previous studies (Imae *et al.*, 2011) and suggest that LYCAT preferentially affects the acyl chain profile of a subset of PIPs, including PI(4,5)P_2, which may be necessary to maintain PI(4,5)P_2 levels, localization, and function.

LYCAT is localized to ER-derived PIS vesicles

Previous studies suggested that LYCAT may exhibit some localization to the ER (Cao *et al.* 2004; Zhao *et al.* 2009; Imae *et al.*, 2011). However, these studies did not perform a broader analysis of LYCAT localization with other relevant markers, an important consideration, since the ER has several subcompartments (English and Voeltz, 2013). We hypothesized that the preferential effect of LYCAT silencing on the acyl chain profile of PI(4,5)P_2 but not PI/PIP_1 may be in part due to its restricted localization to specific cellular subcompartment(s). To monitor LYCAT localization, we transfected RPE cells with LYCAT-FLAG, which rescued the loss of endogenous LYCAT (Figure 1C), demonstrating that this exogenously expressed LYCAT is functional. Of interest, LYCAT-FLAG exhibited modest localization with eGFP-KDEL, a generic ER marker (Figure 6, A and B), suggesting that LYCAT may predominantly localize to other subcompartments.

PIS is found in ER-derived vesicles that rapidly move between the ER and various organelle membranes, as observed in cells expressing eGFP-PIS (Kim *et al.*, 2011). Given the role of PIS in synthesizing PI, we hypothesized that LYCAT may localize to PIS vesicles. We found striking and extensive colocalization between LYCAT and eGFP-PIS (Figure 6, A and B). PIS vesicles make dynamic and transient contact with a number of membrane compartments, including the PM, which can be demarked by the extended synaptotagmin E-Syt2 (Min *et al.*, 2007; Giordano *et al.*, 2013). Indeed, LYCAT exhibited partial colocalization with E-Syt2 (Figure 6, A and B). TIRF-M showed very similar colocalization patterns between LYCAT and PIS, KDEL, and E-Syt2 at the cell periphery (Supplemental Figure S5).

To allow better understanding of the relative localization of LYCAT with eGFP-KDEL, eGFP-PIS, and eGFP-E-Syt2, we analyzed this by automated detection of LYCAT puncta followed by measurement of the localization correlation score (LCS) of the fluorescence intensities of LYCAT and that of secondary channel proteins within each object (Supplemental Figure S6). LCS is a quantitative, unbiased, and systematic analysis and revealed a very strong intensity correlation of LYCAT-FLAG with eGFP-PIS within LYCAT structures (Figure 6B). In contrast, eGFP-KDEL and LYCAT exhibited very low intensity correlation in LYCAT structures, whereas eGFP-E-Syt2 and LYCAT had intermediate intensity correlation (Figure 6B). Thus LYCAT is extensively localized to ER-derived PIS vesicles, known to transiently interact with ER-PM contact sites, but not the ER domains marked by eGFP-KDEL (Kim *et al.*, 2011).

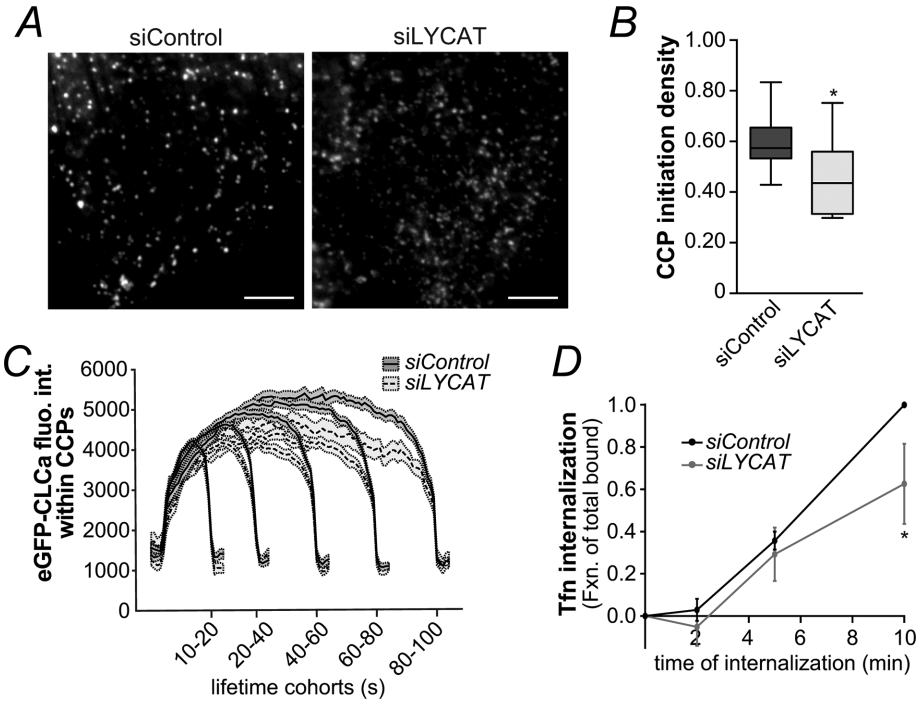

FIGURE 3: LYCAT silencing alters clathrin-mediated endocytosis. RPE cells stably expressing eGFP-CLCa were transfected with siRNA targeting LYCAT (siLYCAT) or nontargeting siRNA (siControl). (A–C) Cells were imaged using time-lapse TIRF-M. (A) Single-frame representative fluorescence micrographs (scale bar, 5 μm). Time-lapse TIRF-M image series were subjected to automated detection, tracking, and analysis of CCPs as described in *Materials and Methods*. (B) Median, 25th and 75th percentiles (boxes), and Tukey range (whiskers) for CCP initiation densities. (C) Mean eGFP-CLCa fluorescence intensity grouped into CCP lifetime cohorts; error bars reflect cell-to-cell variation. The numbers of CCP trajectories and cells for each condition are, for siControl, 7181 and 16, and for siLYCAT, 2354 and 16, respectively. (D) Measurement of Tfn internalization; means ± SEM ($n = 4$), *$p < 0.05$.

DISCUSSION

PIPs play essential roles in cell physiology, including regulation of membrane traffic (Di Paolo and De Camilli, 2006; Krauss and Haucke, 2007). The vast majority of studies on PIPs focused on the regulation and function of the phosphorylation state of the inositol head group. Of importance, PI and PIPs show remarkable acyl selectivity, with 50–70% of PI/PIPs harboring a 1-stearoyl-2-arachidonyl profile (Holub and Kuksis, 1978; Hicks *et al.*, 2006; Imae *et al.*, 2011; D'Souza and Epand, 2014). The function and significance of this acyl selectivity have not been scrutinized at the cell biological level. Here we examine the cell biological function of the PI acyltransferase LYCAT, finding that this enzyme selectively controls the levels, localization, and function of specific PIPs and is localized to dynamic ER-derived vesicles believed to contact the PM. We propose that LYCAT functions simultaneously with or subsequent to PI synthesis to regulate the acyl profile of PI(4,5)P_2, revealing a novel dimension in the regulation of PIP function.

The PI acyltransferase LYCAT preferentially affects the acyl chain profile of PI(4,5)P_2

Acyltransferases may control PI/PIP acylation during de novo synthesis in the ER or by subsequent processes such as acyl or head group remodeling. The de novo synthesis of many phospholipids involves the conversion of DAG to PA (Shindou and Shimizu, 2009). Synthesis of PI results from conversion of PA to CDP-DAG by CDS, followed by conversion to PI by PIS (Shindou and Shimizu, 2009; D'Souza *et al.*, 2014; D'Souza and Epand, 2015). CDS2, but not CDS1 or PIS, exhibits preference for 1-stearoyl-2-arachidonyl substrate, thus providing at least one mechanism for the establishment of acyl specificity of PI during de novo synthesis (D'Souza *et al.*, 2014; D'Souza and Epand, 2015). In addition, PI acyl specificity may occur by acyl remodeling postsynthesis by the joint effort of phospholipases and acyltransferases (Imae *et al.*, 2010). In our LYCAT-silenced cells, we did not observe an alteration in the acyl chain profile of PI or PIP_1, which is chiefly PI(4)P. This suggests that LYCAT may not be acting during bulk PI synthesis or remodeling, although we cannot exclude the possibility that other acyltransferases may act redundantly with LYCAT. On the other hand, there was a significant shift in the acyl chain profile of PIP_2, which is mainly PI(4,5)P_2. Thus LYCAT appears to be part of a pathway that preferentially acts on PI(4,5)P_2 to impart acyl chain selectivity.

How might LYCAT affect the PI(4,5)P_2 acyl profile but not bulk PI/PIP? PI(4,5)P_2 synthesis was classically believed to occur from the sequential conversion of PI to PI(4)P and PI(4,5)P_2 at the PM. However, PI(4,5)P_2 regulation is much more elaborate than this. Rather than depend on general ER or PM, PI and PI(4,5)P_2 synthesis appear highly dependent on ER-PM contact sites and substrate channeling. Nonvesicular transport of PA, DAG, and PI between the ER and PM is also implicated in this process (Chang and Liou, 2015; Kim *et al.*, 2015; Saheki *et al.*, 2016). In addition, PIS was observed on dynamic ER-derived vesicles that make transient contact with a number of organelles, including with the PM (Kim *et al.*, 2011). These observations led Kim *et al.* (2011) to propose that PIS vesicles form PIPEROsomes, which may be involved in the localized synthesis and/or delivery of PI or PIPs at organelle contact sites. The localization of LYCAT with PIS in apparent vesicular structures (Figure 6) suggests that PI acyl remodeling activity may be coupled to PIS activity in these vesicles. For technical reasons related to the study of endogenous PIS, the ER-derived PIS vesicles have only been observed upon overexpression of eGFP-PIS, which is required to observe the localization of this enzyme (Kim *et al.*, 2011). Our observation that LYCAT also localizes to punctate peripheral structures in the presence or absence of eGFP-PIS overexpression (Figure 6) is consistent with the broad formation of ER-derived vesicles under a number of physiologically relevant conditions. However, the cellular condition(s) that lead to formation of ER-derived vesicles harboring PIS and LYCAT and whether PIS vesicles indeed function to deliver lipids and/or synthesize PI by acting in-*trans* on the PM remain to be determined. Although beyond the scope of the present study, future research should examine the dynamics of PIS and LYCAT within the ER and ER-derived vesicles, including how PIS/LYCAT vesicles interact with the plasma membrane (Kim *et al.*, 2011) and how PI transfer proteins are required for acyl chain remodeling (Cockcroft, 2001; Chang and Liou, 2015).

Work by Hammond *et al.* (2012) showed that depletion of bulk PI(4)P from the PM did not reduce PI(4,5)P_2 levels, suggesting that a different pool of PI(4)P is specifically used to generate PI(4,5)P_2.

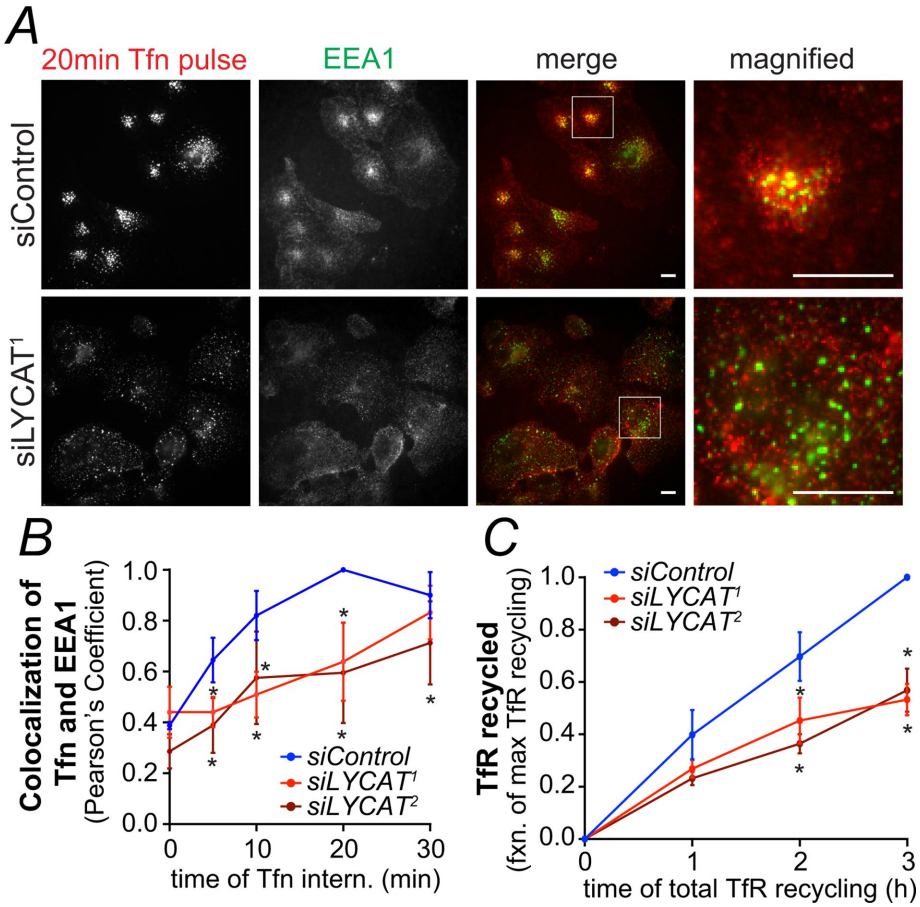

FIGURE 4: LYCAT silencing alters PI(3)P-dependent intracellular TfR membrane traffic. RPE cells were transfected with siRNA targeting LYCAT (siLYCAT) or nontargeting siRNA (siControl). (A, B) Cells were incubated with Tfn-647 for various times and then immediately fixed and stained with EEA1 antibodies. (A) Representative fluorescence micrographs (scale bar, 20 μm). (B) Mean colocalization scores of Tfn and EEA1, normalized to the 20-min control condition, ± SEM ($n = 3$), *$p < 0.05$. (C) Measurement of the rate of TfR recycling; mean TfR recycling ± SEM ($n = 3$), *$p < 0.05$.

Given these emerging themes, we propose the hypothesis that LYCAT acts on a specific PI pool that is channeled toward synthesis of PI(4,5)P_2. In this model, we speculate that PIS generates two pools of PI: 1) PIS in nonspecialized ER membranes generates bulk PI, and 2) PIS and LYCAT, perhaps in distinct subdomains of the ER or in ER-derived vesicles such as PIPEROsomes, regulate a specialized PI pool that is selected for PI(4,5)P_2 synthesis. The role of PIS in total PI synthesis is consistent with reduced levels in total PI, PI(4)P and PI(4,5)P_2 in PIS-silenced cells (Kim *et al.*, 2011). We propose that the newly synthesized PI is then subject to LYCAT-dependent acyl remodeling, resulting in enrichment in 38:x acyl chains, followed by channeling into PI(4)P and PI(4,5)P_2. Although there is no evidence that PI(4)P synthesis is affected by the acyl chains in PI, PIPKIs show preference for PI(4)P substrates containing 38:4 (Shulga *et al.* 2012). Thus, in the absence of LYCAT, there may be an increase in a minor pool of misacylated PI and PI(4)P, the latter being less efficiently converted into PI(4,5)P_2 due to lower PIPKI substrate preference, reducing PI(4,5)P_2 levels.

Of interest, Anderson *et al.* (2013) suggested the existence of a PI-specific Lands cycle upon examination of phospholipids of brains and liver of a mouse knockout of LPIAT1, a PI-specific acyltransferase that exhibits remarkable selectively for incorporation of arachidonic acid into the *sn-2* position of PI. Liver and brains from LPIAT1$^{-/-}$ mice exhibited reduced levels of 38:4 PIP_1 and PIP_2, as well as of total PIP_1 and PIP_2. Taken together with our results, this may suggest a model in which several acyltransferases such as LYCAT and LPIAT1 function in a PI-specific Lands cycle for the synthesis of 38:4 PI, perhaps in a mechanism that involves coordination of several other acyltransferases.

Moreover, the 2xFYVE and PH probes that were used to determine PI(3)P and PI(4,5)P_2 localization and levels may themselves may be selective to the acyl chain profile of the corresponding lipid. As such, it is possible that the altered localization of these probes upon LYCAT silencing may reflect both altered abundance and localization of these PIPs, as well as alterations in their acyl profile. Nonetheless, the biochemical measurements of PI(3)P and PI(4,5)P_2 illustrate that LYCAT silencing indeed affects the levels of both of these lipids.

LYCAT controls clathrin-mediated endocytosis

Previous studies reported that perturbation of PI(4,5)P_2 synthesis resulted in a reduction in CCP initiation rate and size, whereas increased PI(4,5)P_2 synthesis increased CCP initiation rate and size (Antonescu *et al.*, 2011). Our findings that LYCAT perturbation results in reduction in PI(4,5)P_2 levels and a reduction in CCP initiation rate and size are entirely consistent with this previous work. PI(4,5)P_2 functions as a membrane ligand to many CCP proteins, including AP2, epsin, SNX9, CALM, and dynamin (Gaidarov and Keen, 1999; Itoh *et al.*, 2001; Di Paolo and De Camilli, 2006; Krauss and Haucke, 2007; Jackson *et al.*, 2010). Indeed, PI(4,5)P_2 binding to AP2 contributes to conformational changes in AP2, which promotes association with membrane and cargo receptors, thus potentiating CCP assembly (Jackson *et al.*, 2010). Of note, defects in CCP dynamics and endocytosis in LYCAT-silenced cells may result not only from reduced PI(4,5)P_2 levels, but also from a defect in binding to effectors by misacylated PI(4,5)P_2 (van Meer *et al.*, 2008). The acyl chain specificity may be important to dictate the position of the phospholipid head group by controlling the axial position of the lipid in the membrane, affecting membrane curvature, or partitioning of lipids within specific membrane domains. Conversely, or in addition, endocytosis requires turnover of PI(4,5)P_2 from nascent endocytic vesicles catalyzed by synaptojanins and OCRL (Antonescu *et al.*, 2011; Chang-Ileto *et al.*, 2011). Of interest, the OCRL 5-phosphatase activity, and to a lesser extent that of synaptojanin 1, exhibits preference for 1-stearoyl-2-arachidonyl over other acyl profiles in substrates (Schmid *et al.*, 2004). Remarkably, PI(4,5)P_2-labeled tubules and endosomes were present in cells disrupted for 5-phosphatases such as OCRL (Nández *et al.*, 2014), which resembles the appearance of PI(4,5)P_2 in tubules and puncta in cells silenced for LYCAT (Figure 2B). This suggests that misacylated PI(4,5)P_2 may affect endocytosis and be a poor substrate for OCRL/synaptojanins, causing ectopic accumulation of PI(4,5)P_2. It is interesting that LYCAT-knockout mice did not

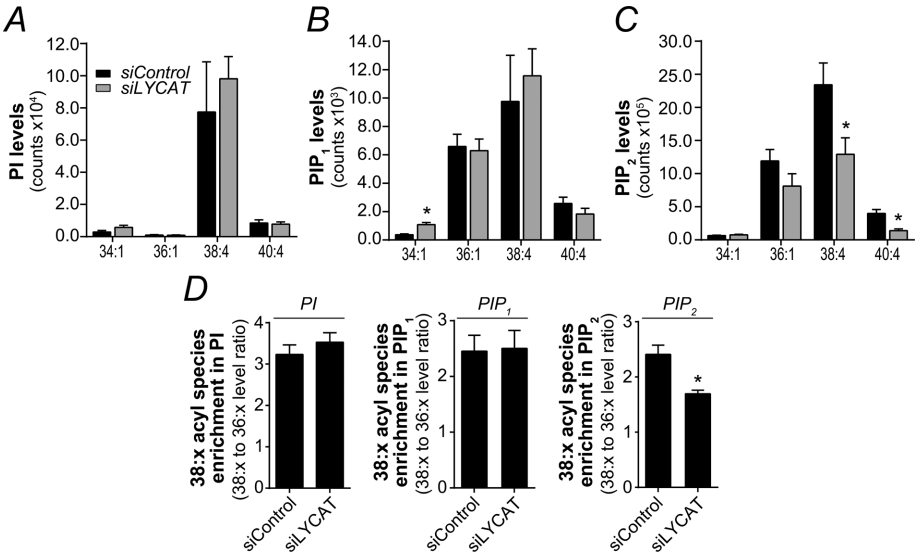

FIGURE 5: LYCAT knockdown alters acyl chain profile of PIP_2 but not that of PI or PIP_1. RPE cells were transfected with siRNA targeting LYCAT (siLYCAT, gray bars) or nontargeting siRNA (siControl; black bars). Cell extracts were subjected to quantitative measurement of acyl group composition of various PIP species by phosphate group methylation, followed by LC-ESI-MS/MS. Means ± SEM of the measurements of molecular compositions of PI (A), PIP_1 (B), and PIP_2 (C). Note that the molecular species indicate the mass and saturation combination of acyl chains on the *sn-1* and *sn-2* positions ($n = 4$); *$p < 0.05$. See Supplemental Figure S4 for additional data related to these measurements. (D) Ratios of the mean 38:*x* to 36:*x* levels in PI, PIP_1 and PIP_2 ($n = 4$), *$p < 0.05$.

show any broad phenotype with respect to viability (Imae *et al.*, 2011). Hence it is likely that there exist compensatory mechanisms for lipid-sensitive processes. Although OCRL and synaptojanin 1 demonstrated preference for substrates with specific acyl profiles, other inositol 5-phosphatases did not (Schmid *et al.*, 2004). Hence long-term perturbation of LYCAT, as it occurs in $LYCAT^{-/-}$ mice, may result in altered expression profile of these lipid phosphatases (or other enzymes) to maintain some of the physiological functions of PIPs under conditions of altered acyl profiles of these lipids.

LYCAT controls PI(3)P and early endosomal traffic

LYCAT suppression resulted in reduced levels of PI(3)P, observed biochemically and using GFP-based probes. There are at least three possible paths to depress PI(3)P levels. First, and as suggested earlier, PI(3)P may depend on a specific precursor PI pool remodeled by LYCAT as we propose for $PI(4,5)P_2$, since PIS vesicles form transient contacts with a number of compartments, including endosomes (Kim *et al.*, 2011). Unfortunately, we cannot currently assess the acyl chain profile of PI(3)P, since this is a minority relative to PI(4)P in the PIP_1 group. Second, defects in $PI(4,5)P_2$ turnover upon LYCAT silencing may affect PI(3)P synthesis. Consistent with this possibility, disruption of early endosomal phosphatases causes a reduction in PI(3)P (Shin *et al.*, 2005). Finally, the effects on PI(3)P levels and PI(3)P-dependent processes may be indirect, resulting from primary defects in clathrin-mediated endocytosis and membrane flux.

Generation of PI(3)P from PI acts as a switch responsible for the maturation of newly formed endocytic vesicles to early endosomes (Zoncu *et al.*, 2009). In addition, depletion of PI(3)P caused these endosomes to revert to the immature endosomes (Zoncu *et al.*, 2009). PI 3-kinase is recruited to the newly formed endosome, where it converts PI into PI(3)P, which, together with the small GTPase Rab5, recruits FYVE domain–containing proteins (including EEA1 and Rabenosyn-5) that are important in sorting events at the early endosome (Christoforidis *et al.*, 1999; Lawe *et al.*, 2000; Nielsen *et al.*, 2000). Our findings that LYCAT silencing causes a reduction in PI(3)P and a reduction in 2FYVE-positive structures are consistent with these known functions of PI(3)P at early endosomes. LYCAT silencing affects the generation of PI(3)P, which in turn affects the recruitment of effectors involved in endosomal traffic. That we did not detect any gross disruption to EEA1 localization is consistent with a study that observed that a proportion of EEA1 remains on early endosomes in Vps34-silenced cells (Johnson *et al.*, 2006). Moreover, EEA1 was strongly recruited to Rab5-positive membranes upon acute depletion of PI(3)P by selective targeting of the PI(3)P phosphatase MTM1 to early endosomes (Fili *et al.*, 2006). Hence some disruptions of PI(3)P production or abundance at the early endosome may allow EEA1 recruitment to early endosomes, perhaps via interaction with Rab5.

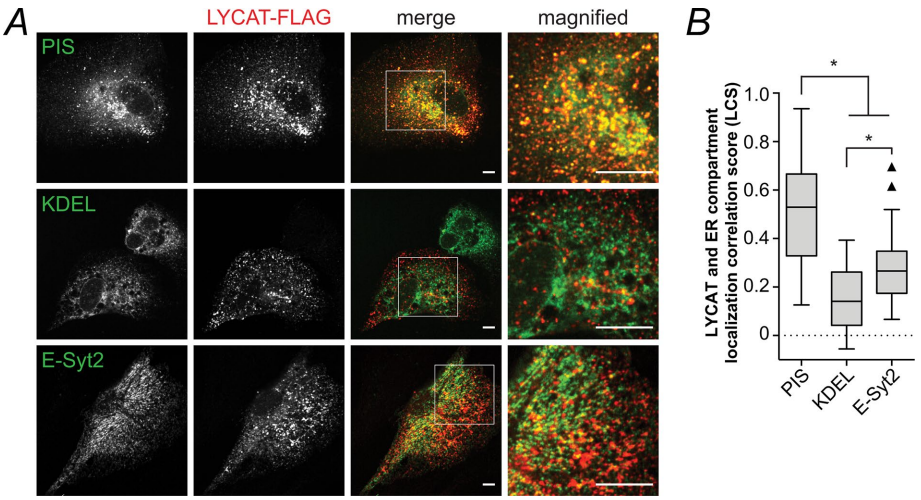

FIGURE 6: LYCAT is localized to ER-derived PIS vesicles. RPE cells were transfected with cDNAs encoding LYCAT-FLAG along with either eGFP-PIS, eGFP-KDEL, or eGFP-E-Syt2 and then subjected to immunofluorescence staining to detect LYCAT-FLAG. (A) Representative epifluorescence micrographs (scale bar, 10 μm). (B) LYCAT-positive structures were subjected to automated detection, followed by measurement of the LCS between LYCAT and eGFP-PIS, eGFP-KDEL, or eGFP-E-Syt2 in these structures. Median, 25th and 75th percentiles (boxes), and Tukey range (whiskers) of LCS values. The numbers of LYCAT structures and cells for each condition are, for eGFP-PIS, 24,907 and 29, for eGFP-KDEL, 14,359 and 24, and for eGFP-E-Syt2, 23,567 and 23, respectively; *$p < 0.05$.

In conclusion, this work adds to the considerable knowledge of how phosphorylation of the inositol head group controls PIP function by revealing that the acyltransferase LYCAT also regulates the dynamics, localization, and function of specific PIPs. These results suggest that control of acyl chain composition of PIPs by dynamic remodeling by specific phospholipases and acyltransferases represent an additional dimension in the control of PI function and suggest that this process may control membrane traffic and cell physiology.

MATERIALS AND METHODS

Materials

DMEM/F12, fetal bovine serum (FBS), penicillin/streptomycin solution, insulin-transferrin-selenium-ethanolamine solution, and sterile 4-(2-hydroxyethyl)-1-piperazineethanesulfonic acid (HEPES) buffer were obtained from Life Technologies (Carlsbad, CA), as was Biotin-xx-Tfn. Avidin and *o*-phenylenediamine hydrochloride reagent were obtained from Biobasic (Markham, Canada), and biocytin was obtained from Santa Cruz Biotechnology (Dallas, TX). Superblock blocking buffer was obtained from Thermo Fisher (Rockford, IL). Antibodies and fluorescent ligands used were as follows: anti-LYCAT from Genetex (Irvine, CA); anti-EEA1 and actin from Cell Signaling Technology (Danvers, MA); anti-TfR from Santa Cruz Biotechnology; Tfn antibodies (used in Tfn uptake assay) from Bethyl Laboratories (Montgomery, TX); and Alexa 647–conjugated Tfn (A647-Tfn) from Life Technologies.

Cell culture, transfection, gene silencing, and Western blotting

Wild-type ARPE-19 (RPE) human retinal pigment epithelial cells (RPE-WT) and a derivative line stably expressing clathrin light chain fused to eGFP (RPE eGFP-CLCa) were previously described (Aguet *et al.*, 2013; Garay *et al.*, 2015). Cells were cultured in DMEM/F12 supplemented with 10% FBS, 100 U/ml penicillin, and 100 µg/ml streptomycin at 37°C and 5% CO_2. A plasmid encoding LYCAT-myc-FLAG (henceforth, LYCAT-FLAG) was from OriGene (plasmid MR226119; Rockville, MD). Plasmids encoding eGFP-PIS and eGFP-P4M were kindly provided by T. Balla (National Institutes of Health, Bethesda, MD; Kim *et al.*, 2011; Hammond *et al.*, 2014). A plasmid encoding eGFP-E-Syt2 (66831; Addgene) was kindly provided by P. de Camilli (Yale School of Medicine, New Haven, CT; Giordano *et al.*, 2013). Plasmids expressing VSVG-GFP protein were previously characterized (Lippincott-Schwartz *et al.*, 1997; Fairn *et al.*, 2011).

For plasmid transfection of RPE cells, we used Lipofectamine 2000 (Life Technologies) as per manufacturer's instructions. For each well of a six-well plate, 2 µg of cDNA was precomplexed with 6 µl of transfection reagent in Opti-MEM. Cells were subsequently incubated with DNA-reagent complexes for 4 h, followed by washing and incubation of cells in regular growth medium for 24 h before the start of the experiment.

To perform LYCAT silencing, we used the following siRNA oligonucleotides (sense) from Dharmacon (Lafayette, CO): LYCAT[1], 5′-GGAAAUGGAAGGAUGACAAUU; LYCAT[2], 5′-CCUCAAAGCGAGUCUCAAAUU; and nontargeting control siRNA, 5′-CGUACUGCUUGCGAUACGGUU. Oligonucleotides were transfected using Lipofectamine RNAiMAX (Life Technologies), as per manufacturer's instructions. Each siRNA construct was transfected at 220 pmol/l precomplexed to the transfection reagent in Opti-MEM for 4 h, after which cells were washed and replaced in regular growth medium. siRNA transfections were performed twice (72 and 48 h) before each experiment.

To confirm LYCAT silencing, whole-cell lysates were prepared in Laemmli sample buffer (LSB; 0.5 M Tris, pH 6.8, glycerol, 10% SDS, 10% β-mercaptoethanol, and 5% bromophenol blue; all from BioShop, Burlington, Canada) supplemented with a protease and phosphatase cocktail (1 mM sodium orthovanadate, 10 nM okadaic acid, and 20 nM Protease Inhibitor Cocktail [BioShop]). Lysates were then heated at 65°C for 15 min and passed through a 27.5-gauge syringe. Proteins were resolved by glycine-Tris SDS–PAGE, followed by transfer onto a polyvinylidene fluoride membrane, and were washed, blocked, and incubated with antibodies as previously described (Garay *et al.*, 2015). Western blot signals to detect the intensity corresponding to LYCAT protein was obtained by signal integration in an area corresponding to the appropriate lane and band for each condition. This measurement is then normalized to the loading control signal (determined with anti-actin antibodies [Cell Signaling Technology]) and subjected to statistical analysis by *t* test.

Immunofluorescence staining

To detect cell surface TfR (Figure 1, A–C), after experimental treatments as indicated, samples were immediately placed on ice and washed three times in ice-cold PBS^{2+} (phosphate-buffered saline supplemented with 1 mM $CaCl_2$ and 1 mM $MgCl_2$) and incubated with anti-TfR antibodies (also on ice; Santa Cruz Biotechnology). After washing to remove unbound antibodies, cells were fixed in 4% paraformaldehyde, permeabilized in 0.1% Triton X-100, stained with appropriate secondary antibodies, and then mounted in fluorescence mounting medium (Dako, Carpinteria, CA).

To detect specific proteins in permeabilized cells (Figures 1, D–F, 2, A and B, and 6 and Supplemental Figures S2A and S5) samples were fixed in 4% paraformaldehyde, permeabilized in 0.1% Triton X-100, probed with appropriate combinations of primary and secondary antibodies, and then mounted in fluorescence mounting medium (Dako).

Fluorescence microscopy

Wide-field epifluorescence microscopy experiments presented in Figures 1, A and D, and 4A and Supplemental Figure S2, A and B, were obtained using a 63× (numerical aperture [NA] 1.2) oil objective on a Zeiss Axiovert 200 M epifluorescence microscope using an ORCA-Flash 4.0 camera (Hamamatsu, Bridgewater, NJ).

Spinning-disk confocal microscopy experiments presented in Figures 2B and 6A were obtained using a Leica DMIRE2 equipped with a Yokogawa CSU X1 scan head and a 60× (NA 1.35) oil objective using a Hamamatsu C9100-13 electron-multiplying charge-coupled device (EM-CCD) camera. Excitation light was provided by 491-nm (50 mV) and 561-nm (50 mW) laser illumination, and emitted light was collected after passage through 515/40 and 594/40-nm emission filters, as appropriate.

Laser scanning confocal microscopy experiments presented in Figure 1F were obtained using a Zeiss LSM700 with a 63× (NA 1.4) oil objective. Excitation light was provided by 488-nm laser illumination.

For TIRF-M, live-cell imaging (Figure 3) was performed on cells incubated in DMEM/F12 lacking phenol red supplemented with 5% fetal bovine serum and oxyrase (1/100; Oxyrase, Mansfield, OH). Cells were placed at 37°C with 5% CO_2. Time-lapse image sequences were acquired at 1-s frame rate. For experiments on fixed cells (Supplemental Figure S5), samples were processed as described in *Immunofluorescence staining*. TIRF-M was performed using a 150× (NA 1.45) objective on an Olympus IX81 instrument equipped with CellTIRF modules (Olympus Canada, Richmond Hill, Canada) using 491-nm (50 mW) and 561-nm (50 mW) laser illumination and 520/35-nm and 624/40-nm emission filters. Images were acquired using a C9100-13 EM-CCD camera.

Fluorescence microscopy image analysis

Quantification of cell surface TfR and internal TfR distribution. Cell surface TfR (Figure 1, B and C) was quantified by measurement of the mean fluorescence intensity over the area of the whole cell. The relative concentration of TfR staining within the perinuclear region (Figure 1, D and E) was measured by kurtosis of a Gaussian model of the TfR staining intensity over the area of the whole cell. Both analyses were performed with ImageJ (National Institutes of Health, Bethesda, MD), and data were normalized to control. Measurements were subjected to *t* test.

Automated detection, tracking, and analysis of CCPs. Time-lapse image series obtained by TIRF-M of cells expressing eGFP-CLCa were subjected to automated detection, tracking, and analysis using custom software in Matlab (MathWorks, Natick, MA; Aguet *et al.*, 2013). Briefly, CCPs were detected using a Gaussian-model based approach to approximate the point spread function, followed by tracking of CCPs through each image series (Jaqaman *et al.*, 2008). Because CCPs are diffraction-limited objects, the amplitude of the Gaussian model of the fluorescence intensity of eGFP-CLCa informs about CCP size (Figure 3C). Given the heterogeneity of CCP lifetimes, for eGFP-CLCa fluorescence intensity measurements of CCP size, objects were separated into lifetime cohorts.

LYCAT localization correlation score. Dual-channel fluorescence micrographs were subjected to automated and unbiased detection of LYCAT structures and subsequent analysis using custom software in Matlab. Determination of the LCS was done by quantifying the correlation of fluorescence intensities of LYCAT and a second compartment marker signal (eGFP-KDEL, eGFP-PIS, or eGFP-E-Syt2) within LYCAT structures. In dual-channel images, LYCAT objects were detected by a Gaussian model–based approach (Aguet *et al.*, 2013; Garay *et al.*, 2015), using only the LYCAT fluorescence channel for initial object detection. Within LYCAT objects, the fluorescence intensity corresponding to the amount of LYCAT or other protein within each object was determined by the amplitude of the Gaussian model in each structure in each channel.

Given the variability of LYCAT and compartment marker expression levels in each cell and image, fluorescence intensity values (f) were rescaled by converting raw fluorescence values to a fluorescence standard score (z) as follows: $z = (f - \mu)/\sigma$, where μ and σ are the mean and SD of fluorescence values of that channel in that particular image, respectively. For each object, the LCS between two channels, z_1 and z_2, was determined as $LCS = 1 - |z_1 - z_2|$.

To validate this method, we examined the LCS measurements in sample images, shown in Supplemental Figure S6, B–D. We performed LCS analysis on a pair of identical images ("model overlap") and the same pair of identical images in which one of the images had undergone spatial randomization (180° rotation; "scrambled channel position"). Before LCS analysis, the correlation of raw pixel intensities of each channel in each detected LYCAT object shows the expected result (Supplemental Figure S6B): virtually total complete correlation between "model overlap" intensities and no correlation between the "scrambled channel position" intensities. Note that the correlation in the "model overlap" images is not perfect despite the images in each channel being identical, as the detection of LYCAT structures by Gaussian model was done assuming two distinct wavelengths for each channel (as per analysis of experimental images, as shown Figure 6), which was not the case in the sample data. Nonetheless, despite the slight offset of the Gaussian model in the secondary channel in the model images, this validation demonstrates the usefulness of this analysis.

A histogram of the calculated LCS values in these image sets (Supplemental Figure S6C) shows that the "model overlap" images have LCS values in the 0.85–1.0 range (close correlation), whereas, as expected, the "scrambled channel position" images have LYCAT puncta with LCS values that span the entire possible range (0–1.0). LCS values were calculated for many "model overlap" and "scrambled channel position" images (Supplemental Figure S6D), showing strong median correlation scores for "model overlap" images (~0.9) and poor correlation (~0.2) for "scrambled channel position" images.

A sample analysis of LYCAT and eGFP-PIS of the images shown in Supplemental Figure S6A shows a strong correlation of raw fluorescence intensities of LYCAT and eGFP-PIS within detected LYCAT objects (Supplemental Figure S6E), as well as an LCS distribution heavily skewed toward high LCS values (Supplemental Figure S6F).

Tfn colocalization with EEA1 or TfR

RPE cells were incubated with 20 µg/ml of A647-Tfn for indicated times at 37°C and then immediately placed on ice and washed three times in ice-cold PBS^{2+} to remove unbound ligand, fixed in 4% paraformaldehyde, permeabilized in 0.1% Triton X-100, stained with either anti-EEA1 (Cell Signaling Technology) or anti-TfR (Santa Cruz Biotechnology) and appropriate secondary antibodies, and then mounted in fluorescence mounting medium (Dako). Colocalization of A647-Tfn with either EEA1 or TfR was performed in ImageJ using Pearson's *r*. The results were subjected to two-way analysis of variance (ANOVA) followed by Bonferonni's multiple comparison posttest.

VSVG biosynthetic membrane traffic assay

RPE cells were transfected with VSVG-GFP and incubated overnight at 40°C. To allow VSVG-GFP to exit the ER and accumulate in the Golgi, the cells were switched to HEPES-buffered DMEM/F12 and incubated at 20°C for 2 h. To visualize secretory vesicles in transit to the PM, after the 20°C block, the cells were transferred to medium prewarmed to 37°C and incubated for 0, 15, 30, 60, or 90 min. After incubation at 37°C for the indicated time points, cells were washed and fixed with 4% paraformaldehyde for 15 min and washed with PBS. The results were subjected to two-way ANOVA followed by Bonferonni's multiple comparison posttest.

TfR recycling assay

TfR recycling (Figure 4C) was measured as previously described for the measurement of recycling of glucose transporters (GLUTs); these assays allow orthogonal measurement of internalization and recycling kinetics (Antonescu *et al.*, 2008; Ishikura *et al.*, 2010). TfR recycling was performed by incubating cells with (0.5 µg/ml) anti-TfR antibodies, which recognize an exofacial epitope on the receptor (Santa Cruz Biotechnology) in serum-free DMEM to cells, for 0, 1, 2, or 3 h at 37°C. This process results in labeling of TfR molecules upon their exposure to the extracellular milieu, as occurs during recycling to the cell surface. Subsequently cells were washed three times in ice-cold PBS^{2+} to remove unbound TfR antibodies, fixed in 4% paraformaldehyde, permeabilized in 0.1% Triton X-100, and then probed with secondary antibodies to detect all anti-TfR antibodies bound during this assay (whether internalized or not). Samples were then mounted in fluorescence mounting medium (Dako). The amount of antibody bound during a given time interval, corresponding to TfR recycling, was normalized to total cell TfR, measured in parallel. All TfR staining intensity measurements were performed with ImageJ. These measurements were subjected to two-way ANOVA followed by Bonferonni's multiple comparison posttest.

Measurement of TfR recycling by this assay involves labeling of TfR upon exposure to the extracellular milieu and does not subsequently distinguish between antibody-bound TfR that undergoes internalization or that which remains at the cell surface (Antonescu *et al.*, 2008; Ishikura *et al.*, 2010). It is possible that surface antibody labeling by TfR is partial (but similarly so in all experimental conditions), such that only a portion of TfRs is antibody labeled at each round of recycling. This may explain why this method of recycling results in longer apparent recycling time for TfR than the ~60 min previously reported (e.g., Klausner *et al.*, 1983; Stein and Sussman, 1986). If this is the case, then conditions in which TfR internalization slowed may exhibit an overestimation of the rate of TfR recycling rate, as each TfR would have a longer cell surface residence time at each round of recycling through the plasma membrane. As such, given that LYCAT internalization is delayed in LYCAT-silenced cells (Figure 3D), the rate of TfR recycling upon LYCAT silencing may be delayed even further than what is apparent by use of this TfR recycling assay (Figure 4C).

Tfn internalization assay

Cells were then incubated with 10 μg/ml biotinylated transferrin (Invitrogen) for the indicated times at 37°C, after which they were immediately placed on ice and washed three times in ice-cold PBS^{2+} to remove excess (unbound) ligand and arrest membrane traffic. Uninternalized (surface-exposed) biotin-Tfn was quenched by sequential incubation with free avidin (3.1 μg/ml) and biocytin (5 μg/ml). Cells were then solubilized in blocking buffer (0.05% Triton X-100 and 0.05% SDS in Superblock solution; Thermo Fisher), and cell lysates were plated onto enzyme-linked immunosorbent assay plates coated with anti-Tfn antibodies and assayed for detectable (internalized) biotin-Tfn using horseradish peroxidase–conjugated streptavidin. Measurements of internalized Tfn were normalized to the total levels of surface ligand binding measured at 4°C, measured in parallel for each condition. The results were subjected to two-way ANOVA followed by Bonferonni's multiple comparison posttest.

[^{3}H]myo-inositol–based detection of PIP levels

RPE cells were incubated for 24 h in inositol-free DMEM (MP Biomedicals, Santa Ana, CA) supplemented with 10 μCi/ml *myo*-[2-3 H(N)] inositol (PerkinElmer Life Sciences, Waltham, MA), 10% FBS, 4 mM L-glutamine, 1× insulin-transferrin-selenium-ethanolamine, 20 mM HEPES, and 1× penicillin/streptomycin. Cells were treated with 600 μl of 4.5% perchloric acid (vol/vol) on ice for 15 min, scraped, and pelleted at 12,000 × *g* for 10 min. Pellets were washed with 1 ml of ice-cold 0.1 M ethylenediaminetetraacetic acid (EDTA) and resuspended in 50 μl of water. Phospholipids were deacylated with 500 μl of a solution of methanol/40% methylamine/1-butanol (45.7% methanol:10.7% methylamine:11.4% 1-butanol [vol/vol]) for 50 min at 53°C. Samples were vacuum-dried and washed twice with water. The dried samples were then resuspended in water, extracted with a solution of 1-butanol/ethyl ether/ethyl formate (20:4:1), vortexed for 5 min, and centrifuged at 12,000 × *g* for 2 min. The bottom aqueous layer was collected and extracted twice more. The aqueous layer was vacuum-dried and resuspended in 50 μl of water. Equal counts of ^{3}H were separated by HPLC (Agilent Technologies, Santa Clara, CA) through an anion exchange 4.6 × 250 mm column (Phenomenex, Torrance, CA) with a flow rate of 1 ml/min and subjected to a gradient of water (buffer A) and 1 M $(NH_4)_2HPO_4$, pH 3.8 (buffer B). The radiolabeled eluant was detected by β-RAM 4 (LabLogic, Brandon, FL) with a 1:2.5 ratio of eluate to scintillant (LabLogic) and analyzed using Laura 4 software. Each of the PIPs was normalized against the parent PI peak. Measurements were subjected to *t* test.

Phospholipid analysis by LC-ESI-MS/MS

Cells were washed in cold PBS, scraped, and then flash frozen. Lipids were extracted by the method of Bligh and Dyer (1959). Phospholipids in lipid extracts quantitated by using the inorganic phosphorus assay. Internal standards (13:0/15:0 PC, PE, PI, and PS) were added to the samples before LC-ESI-MS/MS analysis. The LC-ESI-MS/MS analysis was performed on a Shimadzu Nexera ultra-high-performance liquid chromatography system (Shimadzu, Kyoto, Japan) coupled with a QTRAP 4500 hybrid triple quadrupole linear ion trap mass spectrometer (AB SCIEX, Framingham, MA). Chromatographic separation was performed on an Acquity UPLC HSS T3 column (100 mm × 2.1 mm, 1.8 μm; Waters, Mississauga, ON, Canada) maintained at 40°C using mobile phase A (water/methanol 50/50 [vol/vol] containing 10 mM ammonium acetate and 0.2% acetic acid) and mobile phase B (isopropanol/acetone 50/50 [vol/vol]) in a gradient program (0–3 min: 30% B → 50% B; 3–24 min: 50% B → 90% B; 24–28 min: 30% B) with a flow rate of 0.3 ml/min. Neutral loss scans of 74 and 87 Da in the negative-ion mode were used to detect PC and PS, respectively. Neutral loss scan of 141 Da in the positive-ion mode was used to detect PE. Precursor ion scan of m/z = 241 in the negative-ion mode was used to detect PI. The instrument parameters for negative-ion mode were as follows: curtain gas, 10 psi; collision gas, 7 arbitrary units; ionspray voltage, −4500 V; temperature, 700°C; ion source gas 1, 30 psi; ion source gas 2, 70 psi; declustering potential, −96 V; entrance potential, −10 V; collision energy, −36 V; and collision cell exit potential, −15.4 V. The instrument parameters for positive-ion mode were as follows: curtain gas, 10 psi; collision gas, 7 arbitrary units; ionspray voltage, 4500 V; temperature, 700°C; ion source gas 1, 30 psi; ion source gas 2, 50 psi; declustering potential, 116 V; entrance potential, 10 V; collision energy, 31 V; and collision cell exit potential, 12 V. Quantification was performed by integration of the peak area of the extracted ion chromatograms for each phospholipid species.

Phosphoinositide measurements by phosphate methylation and LC-ESI-MS/MS

Cells (~10^6 cells) were washed with cold PBS, scraped in 1 M HCl, and centrifuged at 15,000 × *g* for 5 min. The pellets were resuspended in 170 μl of water and 750 μl of $CHCl_3$/MeOH/1 M HCl (2:1:0.1 [vol/vol]) and incubated for 5 min at room temperature. To each sample, 725 μl of $CHCl_3$ and 170 μl of 2 M HCl were added, followed by vortexing. After centrifugation at 1500 × *g* for 5 min, the lower phase was collected and washed with 780 μl of prederivatization wash solution (the upper phase of $CHCl_3$/MeOH/0.01 M HCl (2:1:0.75 [vol/vol]). The lipid extracts were derivatized by adding 50 μl of 2 M TMS-diazomethane in hexane. The derivatization was carried out at room temperature for 10 min and stopped by adding 6 μl of glacial acetic acid. The derivatized samples were washed twice with 700 μl of postderivatization wash solution (the upper phase of $CHCl_3$/MeOH/water (2:1:0.75 [vol/vol]). After addition of 100 μl of MeOH/H_2O (9:1 [vol/vol]), the samples were dried under a stream of N_2, dissolved in 80 μl of MeOH, and sonicated briefly. After addition of 20 μl of water, the samples were subjected to LC-ESI-MS/MS analysis. The LC-ESI-MS/MS analysis was performed on a Shimadzu Nexera ultrahigh- performance liquid chromatography system coupled with a QTRAP 4500 hybrid triple quadrupole linear ion trap mass spectrometer. Chromatographic separation was performed on an Acquity UPLC C4 BEH column (100 mm × 2.1 mm, 1.8 μm; Waters) maintained at 40°C using mobile phase A (water containing 0.1% formate) and mobile phase B (acetonitrile containing 0.1% formate) in a gradient program (0–5 min: 45% B; 5–10 min: 45% B → 100% B; 10–15 min: 100% B;

15–16 min: 100% B → 45% B; 16–20 min: 45% B) with a flow rate of 0.1 ml/min. The instrument parameters for positive-ion mode were as follows: curtain gas, 10 psi; collision gas, 7 arbitrary units; ion-spray voltage, 4500 V; temperature, 600°C; ion source gas 1, 30 psi; ion source gas 2, 50 psi; declustering potential, 121 V; entrance potential, 10 V; collision energy, 39 V; and collision cell exit potential, 10 V. Phosphoinositides were identified and quantified by multiple reaction monitoring (MRM). MRM transition parameters are shown in Supplemental Table S1.

For these measurements, an internal standard of 10 ng of 32:0 PIP_2 was added to each sample. However, normalization of lipid counts to this internal standard was impractical due to the increase in 32:0 and 34:0 PIP_2 in lipid samples from LYCAT-silenced cells. That the raw counts of PI and PIP between control and LYCAT-silenced cells are very similar indicates that the differences in abundance of specific acyl species of PIP_2 between these silencing conditions is not due to differences in whole-sample preparation and instead reflects changes in the levels of PIP_2 acyl species relative to the cellular levels of PI and PIP. Indeed, normalization of each PIP_2 acyl species to the amount of 38:4 PI in each control or LYCAT-silenced sample (Supplemental Figure S4, D and E) illustrates the alterations of PIP_2 acyl species levels relative to PI upon LYCAT silencing.

ACKNOWLEDGMENTS

We thank T. Balla for the kind gifts of the plasmids encoding eGFP-PIS and eGFP-P4M and P. de Camilli for the kind gift of the plasmid encoding eGFP-E-Sty2. This work was supported by an Ontario Early Researcher Award, a Canada Research Chair Award, and a Natural Sciences and Engineering Research Council Grant to R.J.B and a Ryerson Health Research Fund Award and an Operating Grant from the Canadian Institutes of Health Research (Grant 125854) to C.N.A. L.N.B was supported in part by an Ontario Graduate Scholarship.

REFERENCES

Aguet F, Antonescu CN, Mettlen M, Schmid SL, Danuser G (2013). Advances in analysis of low signal-to-noise images link dynamin and AP2 to the functions of an endocytic checkpoint. Dev Cell 26, 279–291.

Anderson KE, Kielkowska A, Durrant TN, Juvin V, Clark J, Stephens LR, Hawkins PT (2013). Lysophosphatidylinositol-acyltransferase-1 (LPIAT1) is required to maintain physiological levels of PtdIns and PtdInsP(2) in the mouse. PLoS One 8, e58425.

Antonescu CN, Aguet F, Danuser G, Schmid SL (2011). Phosphatidylinositol-(4,5)-bisphosphate regulates clathrin-coated pit initiation, stabilization, and size. Mol Biol Cell 22, 2588–2600.

Antonescu CN, Randhawa V, Klip A (2008). Dissecting GLUT4 traffic components in L6 myocytes by fluorescence-based, single cell assays. Methods Mol Biol 457, 367–378.

Balla T (2013). Phosphoinositides: tiny lipids with giant impact on cell regulation. Physiol Rev 93, 1019–1137.

Bligh EG, Dyer WJ (1959). A rapid method of total lipid extraction and purification. Can J Biochem Physiol 37, 911–917.

Cao J, Liu Y, Lockwood J, Burn P, Shi Y (2004). A novel cardiolipin-remodeling pathway revealed by a gene encoding an endoplasmic reticulum-associated Acyl-CoA:Lysocardiolipin acyltransferase (ALCAT1) in mouse. J Biol Chem 279, 31727–31734.

Chang C-L, Liou J (2015). Phosphatidylinositol 4,5-bisphosphate homeostasis regulated by Nir2 and Nir3 proteins at endoplasmic reticulum-plasma membrane junctions. J Biol Chem 290, 14289–14301.

Chang-Ileto B, Frere SG, Chan RB, Voronov SV, Roux A, Di Paolo G (2011). Synaptojanin 1-mediated PI(4,5)P2 hydrolysis is modulated by membrane curvature and facilitates membrane fission. Dev Cell 20, 206–218.

Christoforidis S, McBride HM, Burgoyne RD, Zerial M (1999). The Rab5 effector EEA1 is a core component of endosome docking. Nature 397, 621–625.

Clark J, Anderson KE, Juvin V, Smith TS, Karpe F, Wakelam MJO, Stephens LR, Hawkins PT (2011). Quantification of PtdInsP3 molecular species in cells and tissues by mass spectrometry. Nat Methods 8, 267–272.

Cockcroft S (2001). Phosphatidylinositol transfer proteins couple lipid transport to phosphoinositide synthesis. Semin Cell Dev Biol 12, 183–191.

Conner SD, Schmid SL (2003). Regulated portals of entry into the cell. Nature 422, 37–44.

Cremona O, Di Paolo G, Wenk MR, Lüthi A, Kim WT, Takei K, Daniell L, Nemoto Y, Shears SB, Flavell RA, *et al*. (1999). Essential role of phosphoinositide metabolism in synaptic vesicle recycling. Cell 99, 179–188.

Di Paolo G, De Camilli P (2006). Phosphoinositides in cell regulation and membrane dynamics. Nature 443, 651–657.

D'Souza K, Epand RM (2014). Enrichment of phosphatidylinositols with specific acyl chains. Biochim Biophys Acta 1838, 1501–1508.

D'Souza K, Epand RM (2015). The phosphatidylinositol synthase-catalyzed formation of phosphatidylinositol does not exhibit acyl chain specificity. Biochemistry 54, 1151–1153.

D'Souza K, Kim YJ, Balla T, Epand RM (2014). Distinct properties of the two isoforms of CDP-diacylglycerol synthase. Biochemistry 53, 7358–7367.

Dugani CB, Randhawa VK, Cheng AW, Patel N, Klip A (2008). Selective regulation of the perinuclear distribution of glucose transporter 4 (GLUT4) by insulin signals in muscle cells. Eur J Cell Biol 87, 337–351.

English AR, Voeltz GK (2013). Endoplasmic reticulum structure and interconnections with other organelles. Cold Spring Harb Perspect Biol 5, a013227.

Fairn GD, Schieber NL, Ariotti N, Murphy S, Kuerschner L, Webb RI, Grinstein S, Parton RG (2011). High-resolution mapping reveals topologically distinct cellular pools of phosphatidylserine. J Cell Biol 194, 257–275.

Fili N, Calleja V, Woscholski R, Parker PJ, Larijani B (2006). Compartmental signal modulation: Endosomal phosphatidylinositol 3-phosphate controls endosome morphology and selective cargo sorting. Proc Natl Acad Sci USA 103, 15473–15478.

Gaidarov I, Keen JH (1999). Phosphoinositide-AP-2 interactions required for targeting to plasma membrane clathrin-coated pits. J Cell Biol 146, 755–764.

Garay C, Judge G, Lucarelli S, Bautista S, Pandey R, Singh T, Antonescu CN (2015). Epidermal growth factor-stimulated Akt phosphorylation requires clathrin or ErbB2 but not receptor endocytosis. Mol Biol Cell 26, 3504–3519.

Giordano F, Saheki Y, Idevall-Hagren O, Colombo SF, Pirruccello M, Milosevic I, Gracheva EO, Bagriantsev SN, Borgese N, De Camilli P (2013). PI(4,5)P(2)-dependent and Ca(2+)-regulated ER-PM interactions mediated by the extended synaptotagmins. Cell 153, 1494–1509.

Hammond GR, Fischer MJ, Anderson KE, Holdich J, Koteci A, Balla T, Irvine RF (2012). PI4P and PI(4,5)P2 are essential but independent lipid determinants of membrane identity. Science 337, 727–730.

Hammond GR, Machner MP, Balla T (2014). A novel probe for phosphatidylinositol 4-phosphate reveals multiple pools beyond the Golgi. J Cell Biol 205, 113–126.

Hicks AM, DeLong CJ, Thomas MJ, Samuel M, Cui Z (2006). Unique molecular signatures of glycerophospholipid species in different rat tissues analyzed by tandem mass spectrometry. Biochim Biophys Acta 1761, 1022–1029.

Ho CY, Choy CH, Botelho RJ (2016). Radiolabeling and quantification of cellular levels of phosphoinositides by high performance liquid chromatography-coupled flow scintillation. J Vis Exp 107, doi: 10.3791/53529.

Holub BJ, Kuksis A (1978). Metabolism of molecular species of diacylglycerophospholipids. Adv Lipid Res 16, 1–125.

Imae R, Inoue T, Kimura M, Kanamori T, Tomioka NH, Kage-Nakadai E, Mitani S, Arai H (2010). Intracellular phospholipase A1 and acyltransferase, which are involved in Caenorhabditis elegans stem cell divisions, determine the sn-1 fatty acyl chain of phosphatidylinositol. Mol Biol Cell 21, 3114–3124.

Imae R, Inoue T, Nakasaki Y, Uchida Y, Ohba YY, Kono N, Nakanishi H, Sasaki T, Mitani S, Arai H (2011). LYCAT, a homologue of C. elegans acl-8, acl-9 and acl-10, determines the fatty acid composition of phosphatidylinositol in mice. J Lipid Res 53, 335–347.

Ishikura S, Antonescu CN, Klip A (2010). Documenting GLUT4 exocytosis and endocytosis in muscle cell monolayers. Curr Protoc Cell Biol Chapter 15, Unit 15.15.

Itoh T, Koshiba S, Kigawa T, Kikuchi A, Yokoyama S, Takenawa T (2001). Role of the ENTH domain in phosphatidylinositol-4,5-bisphosphate binding and endocytosis. Science 291, 1047–1051.

Jackson LP, Kelly BT, McCoy AJ, Gaffry T, James LC, Collins BM, Höning S, Evans PR, Owen DJ (2010). A large-scale conformational change

couples membrane recruitment to cargo binding in the AP2 clathrin adaptor complex. Cell 141, 1220–1229.
Jaqaman K, Loerke D, Mettlen M, Kuwata H, Grinstein S, Schmid SL, Danuser G (2008). Robust single-particle tracking in live-cell time-lapse sequences. Nat Methods 5, 695–702.
Johnson EE, Overmeyer JH, Gunning WT, Maltese WA (2006). Gene silencing reveals a specific function of hVps34 phosphatidylinositol 3-kinase in late versus early endosomes. J Cell Sci 119, 1219–1232.
Jost M, Simpson F, Kavran JM, Lemmon MA, Schmid SL (1998). Phosphatidylinositol-4,5-bisphosphate is required for endocytic coated vesicle formation. Curr Biol 8, 1399–1402.
Ketel K, Krauss M, Nicot A-S, Puchkov D, Wieffer M, Müller R, Subramanian D, Schultz C, Laporte J, Haucke V (2016). A phosphoinositide conversion mechanism for exit from endosomes. Nature 529, 408–412.
Kim WT, Chang S, Daniell L, Cremona O, Di Paolo G, De Camilli P (2002). Delayed reentry of recycling vesicles into the fusion-competent synaptic vesicle pool in synaptojanin 1 knockout mice. Proc Natl Acad Sci USA 99, 17143–17148.
Kim YJ, Guzman-Hernandez ML, Balla T (2011). A highly dynamic ER-derived phosphatidylinositol-synthesizing organelle supplies phosphoinositides to cellular membranes. Dev Cell 21, 813–824.
Kim YJ, Guzman-Hernandez ML, Wisniewski E, Balla T (2015). Phosphatidylinositol-phosphatidic acid exchange by Nir2 at ER-PM contact sites maintains phosphoinositide signaling competence. Dev Cell 33, 549–561.
Klausner RD, Van Renswoude J, Ashwell G, Kempf C, Schechter AN, Dean A, Bridges KR (1983). Receptor-mediated endocytosis of transferrin in K562 cells. J Biol Chem 258, 4715–4724.
Krauss M, Haucke V (2007). Phosphoinositides: regulators of membrane traffic and protein function. FEBS Lett 581, 2105–2111.
Lawe DC, Patki V, Heller-Harrison R, Lambright D, Corvera S (2000). The FYVE domain of early endosome antigen 1 is required for both phosphatidylinositol 3-phosphate and Rab5 binding. Critical role of this dual interaction for endosomal localization. J Biol Chem 275, 3699–3705.
Li G, D'Souza-Schorey C, Barbieri MA, Roberts RL, Klippel A, Williams LT, Stahl PD (1995). Evidence for phosphatidylinositol 3-kinase as a regulator of endocytosis via activation of Rab5. Proc Natl Acad Sci USA 92, 10207–10211.
Li J, Romestaing C, Han X, Li Y, Hao X, Wu Y, Sun C, Liu X, Jefferson LS, Xiong J, *et al.* (2010). Cardiolipin remodeling by ALCAT1 links oxidative stress and mitochondrial dysfunction to obesity. Cell Metab 12, 154–165.
Lippincott-Schwartz J, Presley JF, Cole NB, Schroer TA, Hirschberg K, Zaal KJM (1997). ER-to-Golgi transport visualized in living cells. Nature 389, 81–85.
McMahon HT, Boucrot E (2011). Molecular mechanism and physiological functions of clathrin-mediated endocytosis. Nat Rev Mol Cell Biol 12, 517–533.
Min SW, Chang WP, Sudhof TC (2007). E-Syts, a family of membranous Ca2+-sensor proteins with multiple C2 domains. Proc Natl Acad Sci USA 104, 3823–3828.
Nakatsu F, Perera RM, Lucast L, Zoncu R, Domin J, Gertler FB, Toomre D, De Camilli P (2010). The inositol 5-phosphatase SHIP2 regulates endocytic clathrin-coated pit dynamics. J Cell Biol 190, 307–315.
Nández R, Balkin DM, Messa M, Liang L, Paradise S, Czapla H, Hein MY, Duncan JS, Mann M, De Camilli P (2014). A role of OCRL in clathrin-coated pit dynamics and uncoating revealed by studies of Lowe syndrome cells. Elife 3, e02975.
Nielsen E, Christoforidis S, Uttenweiler-Joseph S, Miaczynska M, Dewitte F, Wilm M, Hoflack B, Zerial M (2000). Rabenosyn-5, a novel Rab5 effector, is complexed with hVPS45 and recruited to endosomes through a FYVE finger domain. J Cell Biol 151, 601–612.
Posor Y, Eichhorn-Gruenig M, Puchkov D, Schöneberg J, Ullrich A, Lampe A, Müller R, Zarbakhsh S, Gulluni F, Hirsch E, *et al.* (2013). Spatiotemporal control of endocytosis by phosphatidylinositol-3,4-bisphosphate. Nature 499, 233–237.
Presley JF, Cole NB, Schroer TA (1997). ER-to-Golgi transport visualized in living cells. Nature 389, 81–85.
Puchner EM, Walter JM, Kasper R, Huang B, Lim WA (2013). Counting molecules in single organelles with superresolution microscopy allows tracking of the endosome maturation trajectory. Proc Natl Acad Sci USA 110, 16015–16020.
Saheki Y, Bian X, Schauder CM, Sawaki Y, Surma MA, Klose C, Pincet F, Reinisch KM, De Camilli P (2016). Control of plasma membrane lipid homeostasis by the extended synaptotagmins. Nat Cell Biol 18, 504–515.
Schmid AC, Wise HM, Mitchell CA, Nussbaum R, Woscholski R (2004). Type II phosphoinositide 5-phosphatases have unique sensitivities towards fatty acid composition and head group phosphorylation. FEBS Lett 576, 9–13.
Shin H-W, Hayashi M, Christoforidis S, Lacas-Gervais S, Hoepfner S, Wenk MR, Modregger J, Uttenweiler-Joseph S, Wilm M, Nystuen A, *et al.* (2005). An enzymatic cascade of Rab5 effectors regulates phosphoinositide turnover in the endocytic pathway. J Cell Biol 170, 607–618.
Shindou H, Shimizu T (2009). Acyl-CoA:lysophospholipid acyltransferases. J Biol Chem 284, 1–5.
Shulga YV, Anderson RA, Topham MK, Epand RM (2012). Phosphatidylinositol-4-phosphate 5-kinase isoforms exhibit acyl chain selectivity for both substrate and lipid activator. J Biol Chem 287, 35953–35963.
Stauffer TP, Ahn S, Meyer T (1998). Receptor-induced transient reduction in plasma membrane PtdIns(4,5)P2 concentration monitored in living cells. Curr Biol 8, 343–346.
Stein BS, Sussman HH (1986). Demonstration of two distinct transferrin receptor recycling pathways and transferrin-independent receptor internalization in K562 cells. J Biol Chem 261, 10319–10331.
Stenmark H, Aasland R, Driscoll PC (2002). The phosphatidylinositol 3-phosphate-binding FYVE finger. FEBS Lett 513, 77–84.
Stephens LR, Jackson TR, Hawkins PT (1993). Agonist-stimulated synthesis of phosphatidylinositol(3,4,5)-trisphosphate: a new intracellular signalling system?. Biochim Biophys Acta 1179, 27–75.
Szentpetery Z, Várnai P, Balla T (2010). Acute manipulation of Golgi phosphoinositides to assess their importance in cellular trafficking and signaling. Proc Natl Acad Sci USA 107, 8225–8230.
van Dam EM, ten Broeke T, Jansen K, Spijkers P, Stoorvogel W (2002). Endocytosed transferrin receptors recycle via distinct dynamin and phosphatidylinositol 3-kinase-dependent pathways. J Biol Chem 277, 48876–48883.
van Meer G, Voelker DR, Feigenson GW (2008). Membrane lipids: where they are and how they behave. Nat Rev Mol Cell Biol 9, 112–124.
Várnai P, Balla T (1998). Visualization of phosphoinositides that bind pleckstrin homology domains: calcium- and agonist-induced dynamic changes and relationship to myo-[3H]inositol-labeled phosphoinositide pools. J Cell Biol 143, 501–510.
Varnai P, Thyagarajan B, Rohacs T, Balla T (2006). Rapidly inducible changes in phosphatidylinositol 4,5-bisphosphate levels influence multiple regulatory functions of the lipid in intact living cells. J Cell Biol 175, 377–382.
Zhao Y, Chen Y-Q, Li S, Konrad RJ, Cao G (2009). The microsomal cardiolipin remodeling enzyme acyl-CoA lysocardiolipin acyltransferase is an acyltransferase of multiple anionic lysophospholipids. J Lipid Res 50, 945–956.
Zoncu R, Perera RM, Balkin DM, Pirruccello M, Toomre D, De Camilli P (2009). A phosphoinositide switch controls the maturation and signaling properties of APPL endosomes. Cell 136, 1110–1121.
Zoncu R, Perera RM, Sebastian R, Nakatsu F, Chen H, Balla T, Ayala G, Toomre D, De Camilli PV (2007). Loss of endocytic clathrin-coated pits upon acute depletion of phosphatidylinositol 4,5-bisphosphate. Proc Natl Acad Sci USA 104, 3793–3798.